

# Topological jamming of spontaneously knotted polyelectrolyte chains driven through a nanopore

A. Rosa<sup>1,\*</sup>, M. Di Ventura<sup>2</sup>, and C. Micheletti<sup>1,3†</sup>

<sup>1</sup> *SISSA - Scuola Internazionale Superiore di Studi Avanzati, Via Bonomea 265, 34136 Trieste (Italy)*

<sup>2</sup> *Department of Physics, University of California, San Diego, La Jolla, CA 92093-0319*

<sup>3</sup> *CNR-IOM Democritos, Via Bonomea 265, 34136 Trieste (Italy)*

(Dated: August 4, 2021)

The advent of solid state nanodevices allows for interrogating the physico-chemical properties of a polyelectrolyte chain by electrophoretically driving it through a nanopore. Salient dynamical aspects of the translocation process have been recently characterized by theoretical and computational studies of model polymer chains free from self-entanglement. However, sufficiently long equilibrated chains are necessarily knotted. The impact of such topological “defects” on the translocation process is largely unexplored, and is addressed in this study. By using Brownian dynamics simulations on a coarse-grained polyelectrolyte model we show that knots, despite being trapped at the pore entrance, do not *per se* cause the translocation process to jam. Rather, knots introduce an effective friction that increases with the applied force, and practically halts the translocation above a threshold force. The predicted dynamical crossover, which is experimentally verifiable, is of relevance in applicative contexts, such as DNA nanopore sequencing.

PACS numbers: 36.20.Ey, 82.35.Lr, 87.15.A-, 02.10.Kn

Nanopores, namely holes of nanoscale dimensions carved out of biological or solid-state membranes, are increasingly becoming an important tool to probe chemical and physical properties of polymers [1–6]. For instance, polyelectrolytes, such as DNA, can be electrophoretically translocated through a pore and their chemical composition can be inferred either by the ionic current blocked by the DNA strand [7], or from the electrical current measured perpendicular to the DNA backbone [8]. These approaches are being actively investigated because they hold great promise for fast and low-cost DNA sequencing.

However, one of the issues that has received much less attention is related to possible limitations arising from the maximum length of the polymer that can be electrophoretically translocated through a nanopore without obstruction from the inevitable chain self-entanglement (knots). In fact, it is well known that, the incidence of knots increases exponentially with the chain contour length [9], and, in turn, can affect kinetic, mechanical and equilibrium properties of sufficiently long (bio-)polymers [10–19]. A knot in the polymer chain is then an unwanted potential obstruction to its translocation through a pore; much like the knot we customarily make at the end of a sewing thread to prevent it from “translocating” through a threaded piece of cloth.

Motivated by these observations, in this Letter we set out to investigate theoretically and numerically the dynamics of pore translocation of chains whose contour length exceeds by orders of magnitude their persistence length. On the one hand, this allows us to push to unprecedented contour lengths the assessment of the va-

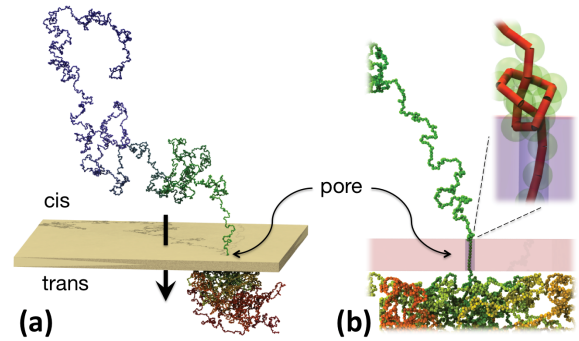


FIG. 1: [Color online] (a) Snapshot of an instantaneous configuration of the  $15\mu\text{m}$ -long model polyelectrolyte driven electrophoretically through the nanopore. The arrow indicates the translocation direction. (b) Cut-through view of configuration in panel (a). The chain backbone, with a tightened trefoil-knot at the pore entrance, is highlighted in the inset.

lidity of previously-suggested dynamical scaling relationships for the translocation process of unknotted chains (see, e.g., Ref. [20–26]). On the other hand, we can clarify the impact of spontaneous knotting on the driven translocation of biopolymers. This avenue appears to be largely unexplored except for the recent protein-related investigation of Huang and Makarov [18].

In particular, we show that knots do not *per se* cause the translocation process to halt. More precisely, they are found to act as plug-like obstructions of the pore only if a threshold driving force is exceeded. Based on this result it is expected that accounting for the topology-dependent dynamical crossover ought to be important for applications that employ nanopores, such as the detection and sequencing of DNA filaments [1, 2].

\*Electronic address: anrosa@sissa.it

†Electronic address: michelet@sissa.it

We consider a model polyelectrolyte chain that is electrophoretically driven through a pore embedded in the slab separating the *cis* and *trans* semi-spaces [1], see Fig. 1. For definiteness, the salient physical properties of the (otherwise general) model system are set to match those of 15 $\mu\text{m}$ -long ssDNA filaments in a solution with 0.1M monovalent salt and translocated through an artificial nanopore. The nominal slab thickness and effective pore diameter were set respectively equal to 10nm and 2nm, consistent with the typical geometry of solid-state nanopores (which are about 3-4 times longer than biological nanopores) [1].

The polyelectrolyte chain consists of  $N = 15000$  beads, with diameter equal to the nominal ssDNA thickness,  $\sigma = 1\text{nm}$ . Because the monovalent counterions reduce the phosphates electrostatic charge by  $\sim 50\%$  [27] the effective charge of the beads, each spanning three nucleotides, is set equal to  $q = -1.5e$ . The chain potential energy is accordingly given by:

$$\mathcal{H} = \sum_{i=1}^N \{U_{\text{FENE}}(d_{i,i+1}) + \frac{1}{2} \sum_{j=1, j \neq i}^N [U_{\text{LJ}}(d_{i,j}) + U_{\text{DH}}(d_{i,j})]\}$$

where  $d_{i,j}$  is the distance of monomers  $i$  and  $j$ , and the three terms, which enforce respectively the chain connectivity constraint ( $U_{\text{FENE}}$ ), the pairwise Lennard-Jones interaction ( $U_{\text{LJ}}$ ) and Debye-Hueckel ( $U_{\text{DH}}$ ) repulsion have the form:

$$U_{\text{FENE}}(d) = \begin{cases} -150\kappa_B T \left(\frac{R_0}{\sigma}\right)^2 \ln \left[1 - \left(\frac{d}{R_0}\right)^2\right], & d \leq R_0 \\ 0, & d > R_0 \end{cases}$$

$$U_{\text{LJ}}(d) = \begin{cases} 4\kappa_B T \epsilon_{i,j} \left[\left(\frac{\sigma}{d}\right)^{12} - \left(\frac{\sigma}{d}\right)^6 + 1/4\right], & d \leq \sigma 2^{1/6} \\ 0, & d > \sigma 2^{1/6} \end{cases}$$

$$U_{\text{DH}}(d) = \frac{q^2 e^{-d/\lambda_{\text{DH}}}}{\epsilon d},$$

where  $R_0 = 1.5\sigma$ ,  $\kappa_B$  is the Boltzmann constant,  $T = 300\text{K}$ ,  $\epsilon = 80$  is the water dielectric constant,  $\lambda_{\text{DH}} = 0.9\text{nm}$  is the Debye screening length, and  $\epsilon_{i,j}$  is equal to 1 if  $|i - j| = 1$ , and 10 otherwise.

A Monte Carlo scheme, employing unrestricted, non topology-preserving local and global moves [28, 29], was first used to generate an equilibrated set of conformations for flexible self-avoiding chains of  $N = 15000$  beads in bulk. The degree and type of entanglement of the filaments was established using the minimally-interfering closure scheme [30, 31]. It was found that  $\sim 2\%$  of the configurations were knotted and, in more than 90% of the cases, they consisted of the simplest knot type: the trefoil or  $3_1$  knot (see inset in Fig. 1b for a trefoil knot representation). The knots spanned, on average, about 10% of the chain; the sizable knot length is consistent with the expected delocalisation of knots in unconstrained chains [32–34].

Since the main focus of the Letter concerns the impact of chain topology on the translocation dynamics, we neglect here the otherwise important issue of how a chain

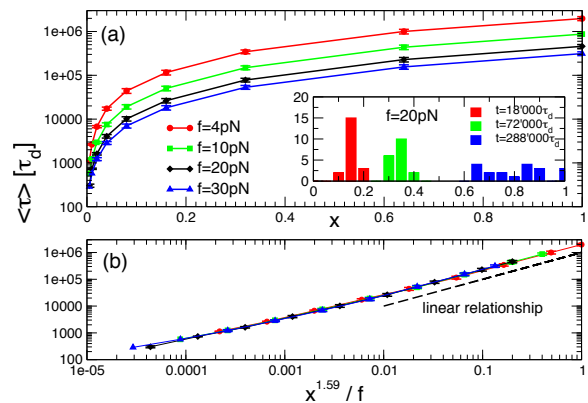


FIG. 2: [Color online] (a) Average time,  $\langle \tau \rangle$ , required to translocate a fraction  $x$  of an unknotted chain at various driving forces,  $f$ . The average is taken over 20 uncorrelated unknotted conformations. Inset: statistical distribution of  $x$  at three different times and  $f = 20\text{pN}$ . Because the process timescale falls in the overdamped regime, time is expressed in units of the nominal monomer self-diffusion time:  $\tau_d = \pi\eta\sigma^3/2\kappa_B T$ . For water viscosity,  $\eta = 1\text{cP}$ ,  $\tau_d \sim 0.5\text{ns}$  [39]. (b) Collapse of the data-points in panel (a) using the theoretical dynamical scaling, see text.

in the bulk approaches the pore and enters it [35]. Accordingly, we extracted from the equilibrated ensemble several uncorrelated knotted and unknotted chains, for which a rigid global translation or rotation could bring one of the ends at the pore entrance while the chain remainder stays in the *cis* semispace.

The beads inside the pore are driven through it by a constant force whose magnitude,  $f$ , typically chosen in the 4 – 40 pN range. Assuming that the electro-osmotic screening inside the channel [6, 36] reduces by  $\sim 50\%$  the charge density of ssDNA, these forces correspond to a uniform electric field of 0.15 – 1.5 V per 10nm acting on each bead. The translocation dynamics of the polyelectrolyte chain is integrated numerically using the fixed-volume and constant-temperature molecular dynamics simulation scheme implemented in the LAMMPS package [37]. As in other coarse-grained approaches, no explicit hydrodynamic treatment is introduced [38].

*Unknotted chain dynamics* - The translocation dynamics for various pulling forces and averaged over an ensemble of 20 *unknotted* chains is illustrated in Fig. 2a. The dynamical process is sensitive to the specific geometrical arrangements of the pulled chains: in fact, the heterogeneity of the process increases with time. As shown in the inset at fixed force and at a given simulation time, the translocated fraction of the chain can range from 50% to 100% depending on the initial configuration. Notwithstanding these differences, the average asymptotic translocation times appear to follow closely the dynamical scaling relationship predicted theoretically,  $\langle \tau \rangle \propto x^{1+\nu}/f$  where  $x$  is the translocated fraction of the chain [20–22]. In fact, by using the theoretical self-avoiding matrix exponent  $\nu = 0.59$ , we find the above

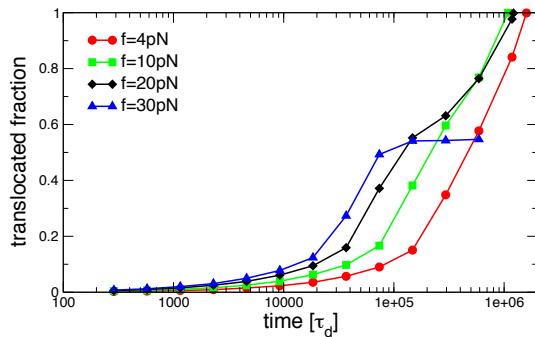


FIG. 3: [Color online] Translocation kinetics of a specific trefoil-knotted chain at various driving forces.

expression well satisfied, see Fig. 2b.

It should also be noted that this scaling relationship, which was first formulated using dimensional and heuristic arguments [20–22], was more recently shown to hold only for asymptotically long chains [26]. In fact the non-equilibrium process that governs the propagation of the tensile disturbance along the chain is sensitive to finite chain effects [26]. The collapse of the data points in Fig. 2b clarify that the theoretically-predicted asymptotic scaling relationship holds satisfactorily for chains of  $N = 15000$  beads with the considered driving protocol.

*Knotted chain dynamics* - Compared to the unknotted case, the translocation dynamics of knotted chains has instead a dramatic, non-monotonic dependence on the driving force. This is illustrated in Fig. 3 for one particular trefoil-knotted configuration where the knot occupies the mid-portion of the chain and spans about 10% of the chain. It is seen that, at the smallest driving force the chain translocation is well-consistent with the average translocation dynamics of unknotted chains. At higher forces, however, the standard dynamic scaling is satisfied only up to when about 50% of the chain is translocated, after which a noticeable slowing down of the process ensues. Notice that at the highest force, the translocation process appears to be practically halted.

This *dynamical crossover* is understood by monitoring the instantaneous position and size of the knot along the chain. The data for  $f = 20pN$  are shown in Fig. 4. It is seen that the knot position along the chain is unperturbed until it is reached by the propagating pulling front. At this stage, the progressive dragging of the chain through the pore causes the knot to tighten. Notice that, because the sequence index of the knot distal end remains about constant in time, the knot tightening process consists of the removal of the “slack” from the end that is nearest to the pore. After this stage, the tightened knot is localized at the pore entrance and the translocation proceeds by chain reptation through the knot “defect”. These results illustrate the remarkable impact that non-trivial *spontaneous entanglement* of long polymer chains has on the translocation dynamics as a function of the pulling force.

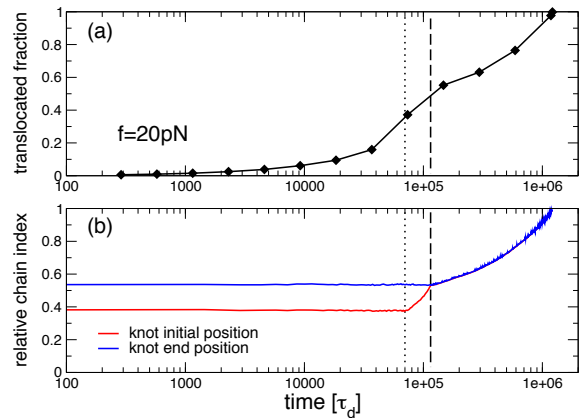


FIG. 4: [Color online] Dynamical evolution (a) of the translocated chain fraction and (b) of the relative knot location along the chain for the same translocation run at  $f = 20pN$  shown in Fig. 3. At time  $t \sim 7 \cdot 10^4 \tau_d$  (dotted line) the propagating pulling front reaches the knot which progressively tightens until it reaches the pore at  $t \approx 1.2 \cdot 10^5 \tau_d$  (dashed line).

To quantify in the most transparent way the topology-dependent aspect of the effect, and separate it from the one associated to the chain geometry we have extended our analysis in two complementary directions. First, by comparing the dynamics of chains with same geometry, but different topology near the pore entrance. Secondly, by suitably averaging the translocation dynamics over chains with different geometry but same knot topology.

For the first analysis, immediately after the knot is tightened at the pore entrance, one can locally perturb the chain geometry at the pore so as to untie the knot, while leaving unaltered the coordinates of all other parts of the chains, see Fig. 5a. Next, by following both the dynamical evolution of the knotted and unknotted versions of the chain (with the same initial velocities for both simulations) it is possible to compare the net effect of the localized knot defect on the chain translocation dynamics. The results are shown in Fig. 5 and aptly illustrate that the slowing down of the translocation process is ascribable to the presence of the localized knot at the pore entrance.

A quantitative assessment of the topology-dependent hindrance can be made by comparing the average translocation times of chains that are unknotted (see Fig. 2a) and of chains whose knot is initially close to the chain end at the pore entrance. Specifically, we considered chains where the knot was located within the first 10-20% of the chain, and for which the knot tightening and trapping occurs within a time span that is typically less than 5% of the full translocation process. We computed the effective friction coefficient,  $\gamma_{knot}$ , of these knot-dominated processes and found that it has a dramatic dependence on  $f$ . This contrasts with the unentangled case where  $\gamma_0$  is practically force-independent, as testified by the collapse of the data in Fig. 2. The effect is illustrated in Fig. 6.

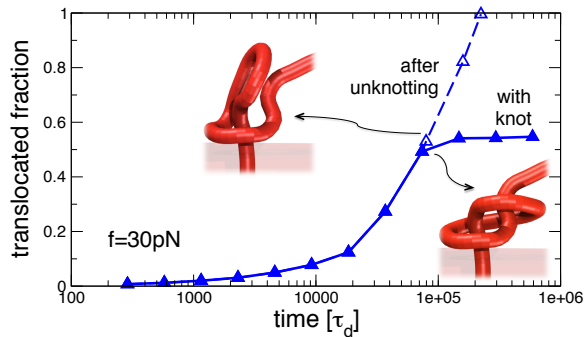


FIG. 5: [Color online] Dependence of the translocation dynamics on the chain topology. After unknotting the chain by the shown local modification of the chain at the pore entrance the translocation velocity is dramatically enhanced. For clarity, here and in Fig. 6 the chain centerline is rendered as a continuous tube with diameter smaller than  $\sigma$ .

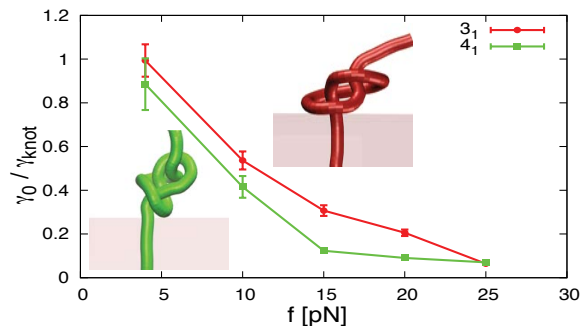


FIG. 6: [Color online] Force dependence of the normalised inverse friction coefficient,  $\gamma_0/\gamma_{knot}$  for chains hosting  $3_1$  knots and  $4_1$  knots. At each force,  $\gamma_0$  is defined as  $\gamma_0 \equiv \langle \tau_i \rangle f / \sigma$ , where  $\langle \tau_i \rangle$  is the average time required by unknotted chains to fully translocate. An analogous definition is used to compute  $\gamma_{knot}$  for  $3_1$ - and  $4_1$ -knotted chains. Averages are taken over 20 configurations for the unknotted case and five configurations for each non-trivial topology.

Notice that at the lowest pulling force,  $f = 4\text{pN}$ , where a fairly tight (spanning 27 monomers on average) knot is trapped at the pore entrance,  $\gamma_{knot}$  is statistically compatible with  $\gamma_0$ . We therefore conclude that knot localization at the pore entrance is not *per se* an impediment

for translocation. It becomes so only when higher pulling forces cause the chain beads to interact very tightly, resulting in a rapidly increasing effective friction. Consistent with the dynamics in Figs. 4 and 5, the trend in Fig. 6 indicates that the translocation process is practically halted at  $f \sim 30\text{pN}$ .

It is interesting to notice that the observed impact of topology on dynamics differs from the case of knotted chains that are passively ejected out of a small spherical cavity [40, 41]. In such systems, knots - even when tight - reduce the ejection speed by only a factor of 2 – 3 [40], possibly due to the relatively small magnitude of the force driving the spontaneous ejection.

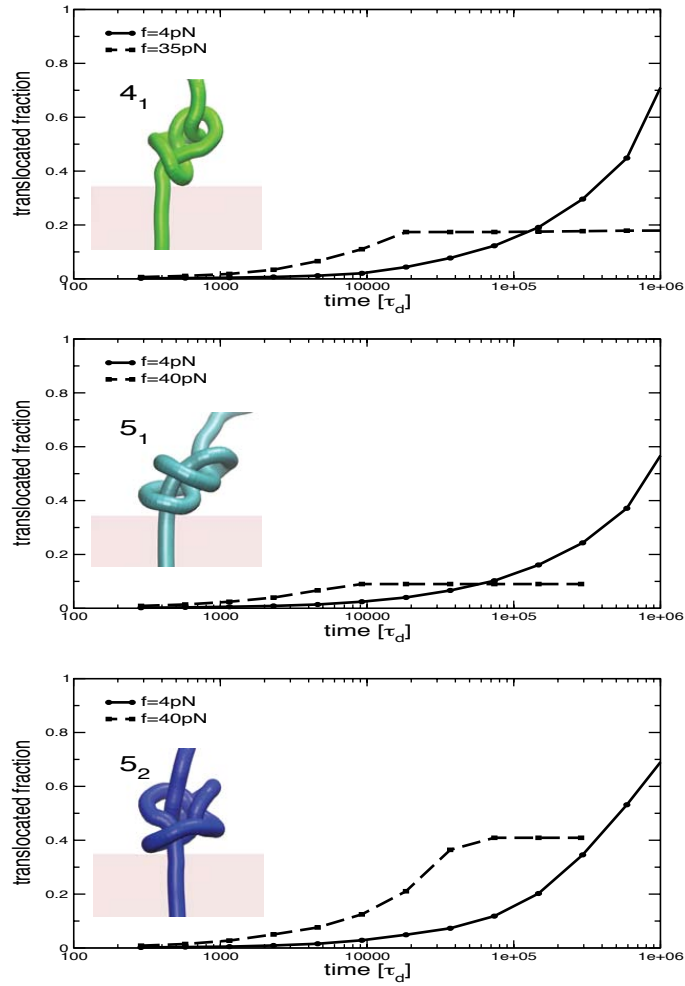
Yet, consistent with available numerical results for knot-controlled DNA ejection [40] and protein translocation dynamics [18] we do observe that at moderate driving forces, the dynamical hindrance is appreciably higher for knots that are more complex (and rarer) than trefoils. In fact, as it is shown in Fig. 6 the average inverse friction coefficient of five  $4_1$ -knotted chains is noticeably smaller than of  $3_1$ -knotted ones. Forces in the 30 – 40pN range are nevertheless sufficient to halt the translocation process of all such  $4_1$ -knotted configurations as well as of five instances of  $5_1$ - and  $5_2$ -knotted ones (see supporting material).

Finally, we stress that the results presented here ought to be relevant in applicative contexts, such as genomic nanopore sequencing where the high-throughput demand pushes towards interrogating longer and longer uninterrupted DNA filaments at pulling forces comparable to those considered in this work [1, 2]. The high-throughput condition inevitably leads to significant chain self-entanglement, while high pulling forces may cause tight knots to halt the translocation process. It should also be pointed out that in actual ssDNA chains the latter effect will expectedly be more severe than in our model system because of both the ramified character of the molecule, and base-pairing effects. Since, the predicted force-dependent topological jamming is experimentally verifiable, we hope that the present investigation will motivate further studies aimed at quantifying this effect.

We acknowledge support from the Italian Ministry of Education and the National Human Genome Research Institute of NIH.

- 
- [1] M. Zwolak and M. Di Ventra, Rev. Mod. Phys. **80**, 141 (2008).  
[2] D. Branton et al., Nat. Biotechnol. **26**, 1146 (2008).  
[3] W. Reisner et al., Phys. Rev. Lett. **94**, 196101 (2005).  
[4] A. J. Storm et al., Nano Letters **5**, 1193 (2005).  
[5] B. Luan and A. Aksimentiev, Soft Matter **6**, 243 (2010).  
[6] S. van Dorp et al., Nat. Phys. **5**, 347 (2009).  
[7] J. J. Kasianowicz et al., Proc. Natl. Acad. Sci. USA **93**, 13770 (1996).  
[8] J. Lagerqvist, M. Zwolak, and M. Di Ventra, Nano Lett. **6**, 779 (2006).  
[9] D. W. Sumners, S. G. Whittington, J. Phys. A: Math. Gen. **21**, 1689 (1988).  
[10] E. Ercolini et al., Phys. Rev. Lett. **98**, 058102 (2007).  
[11] D. Marenduzzo, C. Micheletti, and E. Orlandini, J. Phys.: Condens. Matter **22**, 283102 (2010).  
[12] V. V. Rybenkov, N. R. Cozzarelli, and A. V. Vologodskii, Proc. Natl. Acad. Sci. USA **90**, 5307 (1993).  
[13] A. M. Saitta et al., Nature **399**, 46 (1999).  
[14] Z. R. Liu et al., Nucleic Acids Res. **37**, 661 (2009).  
[15] T. Deguchi and K. Tsurusaki, J. Phys. Soc. Japan **62**, 1411 (1993).

- [16] X. R. Bao, H. J. Lee, and S. R. Quake, *Phys. Rev. Lett.* **91**, 265506 (2003).
- [17] J. I. Sulkowska et al., *Phys. Rev. Lett.* **100**, 058106 (2008).
- [18] L. Huang and D. E. Makarov, *J. Chem. Phys.* **129**, 121107 (2008).
- [19] D. Meluzzi, D. E. Smith, and G. Arya, *Annu. Rev. Biophys.* **39**, 349 (2010).
- [20] Y. Kantor and M. Kardar, *Phys. Rev. E* **69**, 021806 (2004).
- [21] C. Chatelain, Y. Kantor, and M. Kardar, *Phys. Rev. E* **78**, 021129 (2008).
- [22] A. Y. Grosberg et al., *Phys. Rev. Lett.* **96**, 228105 (2006).
- [23] T. Sakaue, *Phys. Rev. E* **76**, 021803 (2007).
- [24] T. Sakaue and E. Raphaël, *Macromolecules* **39**, 2621 (2006).
- [25] C. Forrey and M. Muthukumar, *J. Chem. Phys.* **127**, 015102 (2007).
- [26] T. Ikonen, A. Bhattacharya, T. Ala-Nissila, and W. Sung, *Phys. Rev. E* **85**, 051803 (2012).
- [27] C. Maffeo et al., *Phys. Rev. Lett.* **105**, 158101 (2010).
- [28] N. Madras, A. D. Sokal, *J. Stat. Phys.* **50**, 109 (1988).
- [29] C. Micheletti, D. Marenduzzo, and E. Orlandini, *Phys. Reports* **504**, 1 (2011).
- [30] L. Tubiana, E. Orlandini, and C. Micheletti, *Prog. Theor. Phys.* **191**, 192 (2011).
- [31] L. Tubiana, E. Orlandini, and C. Micheletti, *Phys. Rev. Lett.* **107**, 188302 (2011).
- [32] B. Marcone et al., *Phys. Rev. E* **75**, 041105 (2007).
- [33] P. Virnau, Y. Kantor, and M. Kardar, *J. Am. Chem. Soc.* **127**, 15102 (2005).
- [34] M. L. Mansfield and J. F. Douglas, *J. Chem. Phys.* **133**, 044903 (2010).
- [35] M. Muthukumar, *J. Chem. Phys.* **132**, 195101 (2010).
- [36] B. Luan and A. Aksimentiev, *Phys. Rev. E* **78**, 021912 (2008).
- [37] S. Plimpton, *J. Comp. Phys.* **117**, 119 (1995).
- [38] I. Ali and J. M. Yeomans, *J. Chem. Phys.* **123**, 234903 (2005).
- [39] K. Kremer and G. S. Grest, *J. Chem. Phys.* **92**, 5057 (1990).
- [40] R. Matthews, A. A. Louis, and J. M. Yeomans, *Phys. Rev. Lett.* **102**, 088101 (2009).
- [41] D. Marenduzzo et al., *Proc. Natl. Acad. Sci. USA* **106**, 22269 (2009).



SUPPORTING FIG. 1: Translocation kinetics at low and high force for polymer chains with three different knot topologies  $4_1$ ,  $5_1$  and  $5_2$  as shown in the insets. At low force,  $f = 4\text{pN}$ , the translocation proceeds steadily but it is stalled at  $f \approx 35\text{pN}$  for the  $4_1$ -knotted chain and  $f \approx 40\text{pN}$  for  $5_1$ - and  $5_2$ -knotted chains. The jamming force shown in the examples is typical: 5 instances of  $4_1$  knots were all jammed at  $f = 35\text{pN}$  and 5 instances of five-crossing knots were all jammed at  $f = 40\text{pN}$ . A time step as small as  $0.003\tau_{LJ}$ , ( $\tau_{LJ} = \sigma\sqrt{m}/\epsilon$  is the Lennard-Jones time associated to monomer dynamics [39]) was used to avoid chain breaking due to the build-up of tensile strain in jammed configurations. The default LAMMPS parametrization [39]  $\eta = \frac{\sqrt{m\epsilon}}{6\pi\sigma^2}$  implies that the effective bead mass,  $m$  is  $\approx 2.5 \cdot 10^{-19}\text{kg}$ . We recall in fact that  $\epsilon = \kappa_B T$  ( $\kappa_B$  is the Boltzmann constant and  $T = 300\text{K}$ ),  $\sigma = 1\text{nm}$ , and  $\eta = 1\text{cP}$ . With this effective bead mass,  $\tau_{MD}$  corresponds to  $\approx 6\text{ns}$ . By analysing the velocity-velocity autocorrelation function for internal chain beads, it is established that the overdamped Langevin regime sets in at time-scales  $\approx 0.5\text{ns}$ , i.e. comparable to  $\tau_d$ . In our analysis we accordingly focused exclusively on the mass-independent MD evolution over time-spans longer than  $\tau_d$  and have accordingly expressed time-scales in units of  $\tau_d$ .